

Catalysis Science & Technology

Accepted Manuscript



This is an *Accepted Manuscript*, which has been through the Royal Society of Chemistry peer review process and has been accepted for publication.

Accepted Manuscripts are published online shortly after acceptance, before technical editing, formatting and proof reading. Using this free service, authors can make their results available to the community, in citable form, before we publish the edited article. We will replace this *Accepted Manuscript* with the edited and formatted *Advance Article* as soon as it is available.

You can find more information about *Accepted Manuscripts* in the [Information for Authors](#).

Please note that technical editing may introduce minor changes to the text and/or graphics, which may alter content. The journal's standard [Terms & Conditions](#) and the [Ethical guidelines](#) still apply. In no event shall the Royal Society of Chemistry be held responsible for any errors or omissions in this *Accepted Manuscript* or any consequences arising from the use of any information it contains.

Unique Reaction Mechanism of Preferential Oxidation of CO over Intermetallic Pt₃Co Catalysts: Surface-OH-Mediated Formation of Bicarbonate Intermediate

Shinya Furukawa, Kengo Ehara, and Takayuki Komatsu*

Department of Chemistry, Tokyo Institute of Technology, 2-12-1-E1-10 Ookayama, Meguro-ku, Tokyo 152-8551, Japan

Corresponding authors

Takayuki Komatsu

Department of Chemistry, Tokyo Institute of Technology, 2-12-1-E1-10 Ookayama, Meguro-ku, Tokyo 152-8551, Japan

E-mail: komatsu.t.ad@m.titech.ac.jp, Tel: +81-3-5734-3532, Fax: +81-3-5734-2758

Abstract

A mechanistic study was performed regarding the preferential oxidation of CO in excess H₂ (PROX) over a Pt₃Co intermetallic compound supported on various metal oxides (Pt₃Co/MO_x: MO_x = SiO₂, Al₂O₃, MgO, CaO, and La₂O₃). Pt₃Co/MgO catalyst exhibited the highest catalytic activity (97% CO conversion at 100°C). CO chemisorption revealed that (1) Pt dispersion differed depending on the nature of the support and preparation conditions and (2) catalytic activity strongly depended on Pt dispersion but not on the acid-base properties of the support. A kinetic study suggested that CO and O₂ adsorbed competitively on Co sites. In situ Fourier transform infrared analysis using D₂ indicated that, at a low temperature (< 60°C), a bicarbonate species was formed as a reaction intermediate from CO, O₂, and hydrogen that was supplied from the surface hydroxyl groups, not gas phase H₂, followed by its decomposition to CO₂ and H₂O in a 1:1 ratio. At a high temperature (> 80°C), gas phase H₂ is likely to participate in the formation of the bicarbonate-like intermediate. This study provides the first spectroscopic evidences of bicarbonate formation as an intermediate and the contribution of surface hydroxyl groups toward catalysis. The proposed reaction mechanism based on bicarbonate formation is unique compared with those reported for other PROX systems.

Keywords: Pt₃Co; PROX; intermetallic compound; bicarbonate; mechanistic study

Introduction

The preferential oxidation of CO (PROX) in excess H₂ is a very important reaction for the removal of residual CO in crude hydrogen, which otherwise fatally deactivates Pt electrodes in polymer electrolyte fuel cells (PEFCs).¹ However, it remains an attractive and challenging task to attain both high catalytic activity under mild conditions close to the working temperature of PEFCs (approximately 100°C) and high selectivity for CO oxidation over H₂ combustion. To date, various Pt-based bimetallic materials have been reported as effective catalysts for PROX by many researchers, including us.²⁻¹⁹ The second element is typically a late 3d transition metal (Mn,² Fe,³⁻⁹ Co,¹⁰⁻¹⁴ Cu,¹⁴⁻¹⁸ or Ni¹⁹) present in various states such as oxides,^{2, 3, 8, 12, 15, 18} alloys,^{4, 5, 9, 13} or intermetallic compounds.^{10, 14-17} The most commonly accepted interpretation for their high catalytic activities at low temperature is that the second metal acts as an adsorption site for O₂.²⁰ a kinetically favored Langmuir–Hinshelwood-type association of CO and an oxygen species is permitted in the presence of O₂ adsorption sites, whereas an Eley–Rideal association is imposed in the absence of such sites because of the strong adsorption of CO on the Pt surface. An O₂ supply to the catalyst surface could also be achieved using ceria-based reducible oxides such as CeO₂^{8, 21, 22}, Ti_xCe_(1-x)O₂²³ or CeO₂–ZrO₂.²⁴ However, regardless of the vast amount of research, very few studies have attempted to determine a detailed reaction mechanism including the nature of the reaction intermediates. Understanding the mechanism of Pt-catalyzed PROX would be advantageous not only for establishing the chemistry of this reaction but also for developing more efficient catalysts.

We previously reported that intermetallic Pt₃Co nanoparticles supported on SiO₂ exhibited much higher CO conversion than that in monometallic Pt/SiO₂.¹⁴ Intermetallic compounds have specific crystal structures and ordered atomic arrangements; therefore, the metallic surface predominantly comprises of the Pt–Co interface, at an atomic level, which provides an ideal reaction site for PROX. Furthermore, the ordered atomic arrangement simplifies the discussion regarding the reaction environment and mechanism.

In the present study, we performed a detailed mechanistic study on the nature of PROX over Pt₃Co catalysts on various oxide supports. Several approaches combined with isotope experiments and the in situ Fourier transform infrared (FT-IR) characterization were applied to determine the stepwise reaction mechanism. The effect of the catalyst support on the mechanism was also investigated. Herein, we

demonstrate a unique reaction mechanism for PROX that is strongly supported by spectroscopic evidence.

Experimental Section

Catalyst Preparation

Supported Pt₃Co catalysts (Pt 3 wt%, Pt/Co = 3) were prepared via a co-impregnation method using a mixed aqueous solution of Pt and Co salts. As the catalyst support, either SiO₂ (Cariact G-6, Fuji Silysia Co., $S_{\text{BET}} = 640 \text{ m}^2\text{g}^{-1}$), Al₂O₃ (JRC-ALO-8, $\gamma + \theta$ phase, $S_{\text{BET}} = 250 \text{ m}^2\text{g}^{-1}$), TiO₂ (JRC-TIO-7, anatase, $S_{\text{BET}} = 120 \text{ m}^2\text{g}^{-1}$), La₂O₃ (Kanto, 99%, $S_{\text{BET}} = 1.9 \text{ m}^2\text{g}^{-1}$), CaO (Wako, 99%, $S_{\text{BET}} = 3.6 \text{ m}^2\text{g}^{-1}$), or MgO (UBE Materials, $S_{\text{BET}} = 28\text{--}38 \text{ m}^2\text{g}^{-1}$) were used. CaO was hydrated in water at 80°C for 2 h, followed by drying and calcination under Ar flow ($60 \text{ mL}\cdot\text{min}^{-1}$) at 500°C for 2 h. This procedure significantly increased the specific surface area ($S_{\text{BET}} = 37 \text{ m}^2\text{g}^{-1}$). Two kinds of SiO₂-supported catalysts were prepared using pore-filling impregnation. (1, designated by SiO₂-a) The mixed aqueous solution of Pt(NH₃)₄(OCOCH₃)₂·H₂O and Co(NO₃)₃·6H₂O was added dropwise to dried silica gel such that the solution just filled the pore. The mixture was then dried on a hot plate, followed by reduction under hydrogen flow ($60 \text{ mL}\cdot\text{min}^{-1}$, 99.9995%, Taiyo Nippon Sanso) at 600°C for 2 h. (2, designated by SiO₂-b) HPtCl₆·6H₂O was used instead of Pt(NH₃)₄(OCOCH₃)₂·H₂O, followed by a procedure similar to (1) with calcination at 400°C for 3 h prior to reduction. Other supported catalysts were prepared by the impregnation of an aqueous mixture of HPtCl₆·6H₂O and Co(NO₃)₃·6H₂O to an aqueous slurry of the support without calcination. The reduction was performed at either 600°C (TiO₂), 800°C (Al₂O₃, MgO, La₂O₃, H-ZSM-5), or 900°C (CaO) for 2 h.

PROX Reaction

PROX reaction was carried out in a fixed-bed continuous flow reactor under atmospheric pressure. A specific amount (0.050 g) of catalyst was mixed with α -alumina (0.1 g) and placed in a 17-mm ID quartz tubular reactor. Prior to the catalytic reaction, the catalyst was reduced under hydrogen flow at 400°C for 30 min and purged under helium flow at 400°C. The reaction was initiated at 60°C by supplying a

reactant gas composed of CO (2.0%), O₂ (2.0%), H₂ (35%), and He (balance) with a total flow rate of 135 mL min⁻¹. The reaction temperature was increased stepwise with product analysis at each temperature. Gaseous products were analyzed using an online thermal conductivity detection gas chromatograph (Shimadzu, GC-8A) with an active carbon column (2 mm ID, 3 m length, GL Science). At each temperature, analysis was repeated until the CO conversion reached a constant value. The final values were reported. CO₂ selectivity was calculated based on the total amount of oxygen converted to CO₂ and H₂O. A kinetic study was performed at 60°C, where CO conversion was below 25%, by changing pressure of CO (P_{CO}) and O₂ (P_{O_2}). The reaction rate (r) was defined as follows: r [mL·min⁻¹·g⁻¹] = $F \times x / W$, where F , x , and W are feeding rate, CO conversion, and catalyst amount. The reaction orders of P_{CO} and P_{O_2} were estimated by the slopes of $\ln r - \ln P_{\text{CO}}$ and $\ln r - \ln P_{\text{O}_2}$ plots, respectively. A transient experiment with H₂ on/off treatments was also performed at 100°C. PROX and CO oxidation were switched with short intervals by shutting and resuming the H₂ supply.

Characterization

The crystal structures of the catalysts were examined by powder X-ray diffraction (XRD) with a Rigaku RINT2400 diffractometer using a Cu K α X-ray source. In the case of Pt₃Co/Al₂O₃, difference XRD pattern was obtained by the subtraction of the Al₂O₃ support pattern from that of Pt₃Co/Al₂O₃. Transmission electron microscopy (TEM) was conducted on a JEOL JEM-2010F microscope at an accelerating voltage of 200 kV. In order to prepare the TEM specimens, all samples were sonicated in carbon tetrachloride and dispersed on copper grids supported by an ultrathin carbon film. For the observed nanoparticles in a TEM image, a volume averaged particle (d_{TEM}) size was estimated as a mean particle size defined as the following equation:

$$d_{\text{TEM}} = \frac{\sum_i n_i d_i^4}{\sum_i n_i d_i^3}$$

where, d_i and n_i represent the particle sizes and the number of particles of which sizes are d_i , respectively.

CO pulse chemisorption was carried out at room temperature to estimate the Pt dispersion. One-to-one adsorption of CO on Pt was assumed. Temperature-programmed desorption (TPD) of CO or CO₂ was carried out in a glass circulation system equipped with a vacuum line and a Quadrupole Mass Spectrometer (Spectra International, MICROVISION). Pt₃Co/SiO₂-b (100 mg, for CO) or Pt₃Co/MgO (50 mg, for CO₂) was reduced under flowing hydrogen (60 mL·min⁻¹) at 400°C for 0.5 h, followed by He flowing (60 mL·min⁻¹) and cooling to room temperature. Then the sample was exposed to CO or CO₂ at room temperature, followed by evacuation. The heating rate was set to 5 (CO) or 10 °Cmin⁻¹ (CO₂). FT-IR spectra of surface species over Pt₃Co/MgO were obtained under in situ conditions with a JASCO FT/IR-430 spectrometer in transmission mode. A self-supporting wafer (50 mg·cm⁻²) of the catalyst was placed in a quartz cell with CaF₂ windows and attached to a glass circulation system. The catalyst was reduced under H₂ or D₂ flow at 400°C for 0.5 h, evacuated at the same temperature for 0.5 h, and cooled to room temperature. We confirmed that no surface species other than surface hydroxyl group was detected with the as-pretreated catalyst. After pretreatment, a spectrum was recorded as a baseline for subsequent measurements. The reaction was started at room temperature by introducing the reaction mixture (CO and O₂: 0.5 kPa, H₂ or D₂: 3 kPa). All spectra were recorded at a 1 cm⁻¹ resolution.

Results and Discussion

A series of Pt₃Co catalysts supported on various metal oxides (Pt₃Co/MO_x, M = Si, Al, Mg, Ca, and La) were prepared via an impregnation method. The metallic phases of the prepared Pt₃Co catalysts were analyzed by XRD. As shown in Figure 1, for all catalysts, Pt₃Co was formed in almost a single phase without any other metallic phases that were XRD-observable. The estimated crystallite sizes of Pt₃Co nanoparticles are listed in Table 1. Al₂O₃ and MgO afforded relatively small crystallite sizes (< 7 nm), whereas CaO (18 nm) and La₂O₃ (30 nm) gave larger sizes. For the silica-supported catalysts, Pt₃Co nanoparticles with different crystallite sizes were obtained by changing the preparation method; with (SiO₂-a, 2 nm) or without (SiO₂-b, 7 nm) calcination prior to reduction. This is most likely because oxide phases formed by calcination favor highly dispersed states because of their lower surface energies than those of metallic phases.^{25, 26} Figures 2a–d show the TEM images and size distributions of Pt₃Co supported on SiO₂ (-a and -b), Al₂O₃, and MgO. For silica-supported catalysts, SiO₂-a resulted in a

smaller particle size and narrower size distribution than SiO₂-b. The volume average particle sizes (d_{TEM}) for Pt₃Co/SiO₂-a and -b were 2.8 and 7.4 nm, respectively (Table 1), which are consistent with the crystallite sizes mentioned above. Good agreement with the crystallite size was also observed for Pt₃Co/Al₂O₃ and Pt₃Co/MgO (approximately 6 nm: Figure 2c, 2d, and Table 1). Figure 2e shows the magnification of a single nanoparticle on MgO, designated by a square in Figure 2d. A polyhedral shape with lattice fringes of 2.23 Å spacing was observed, which agrees with that of Pt₃Co(111) planes (2.22 Å, Figure 2f). The crystal shape and fringe direction are also consistent with those of the Pt₃Co cuboctahedron viewed along the [35-2] direction.

The number of exposed Pt atoms on the Pt₃Co nanoparticle surface was estimated by CO chemisorption for the SiO₂-, Al₂O₃-, and MgO-supported catalysts (Table 1). The highest Pt dispersion was obtained with MgO (D_{CO} : 16.0%), followed by Al₂O₃ (D_{CO} : 13.5%). These values slightly exceeded the dispersions calculated based on d_{TEM} and the cuboctahedron model (D_{TEM}). This indicates that the Pt₃Co particles on MgO and Al₂O₃ have slightly Pt-rich surfaces. Conversely, the D_{CO} values for SiO₂-supported catalysts were lower than the D_{TEM} values for both preparation methods (a and b, entries 1 and 2), implying the presence of Co-rich surfaces. SiO₂-a gave larger D_{CO} values than SiO₂-b, most likely because of its small particle size. For Pt-3d-metal alloy nanoparticles, it is known that Pt skins tend to form on the outermost layer after annealing.^{27, 28} However, our results indicate that the surface Pt-Co composition of the supported Pt₃Co particles differs depending on the support. La₂O₃ and CaO gave very low dispersion (< 1%), as anticipated by the large d_{XRD} size. No apparent correlation between the Pt dispersion and surface area of the support was observed (Table 1). Thus, in the present study, Pt dispersion strongly depends on both the nature of the support and preparation method. We also performed a CO-TPD experiment for Pt₃Co/SiO₂-b catalyst to confirm the enrichment of Co on the surface (Figure S1). In a low temperature region (<300°C), two desorption peaks were observed at 85°C and 150°C. These agreed with the reported desorption temperatures of CO molecularly adsorbed on Co and Pt sites of Pt-Co alloys, respectively.²⁹ Note that the lower temperature of desorption from Co indicates the weaker adsorption. The peak intensities of desorption from Pt and Co were comparable despite the bulk composition (Pt/Co = 3.0). This result is very similar to that of Co-rich Pt-Co alloy (Pt/Co = 0.25) in the literature,²⁹ demonstrating the enrichment of Co on the surface of Pt₃Co/SiO₂-b.

We subsequently compared the catalytic performances of the prepared Pt₃Co catalysts in PROX. Figure 3a shows the CO conversions in PROX over various Pt₃Co catalysts as a function of reaction temperature. For all catalysts, CO conversion was increased by elevating the temperature. The order of catalytic activity was as follows: MgO > SiO₂-a > Al₂O₃ > SiO₂-b >> La₂O₃ > CaO, which agrees with the order of Pt dispersion (Figure 3b). In the present study, we employed an activity scale (T_{50}), which represents the temperature at which CO conversion reaches 50% (note that lower T_{50} values reflect higher catalytic activity). The relationship between T_{50} and D_{CO} for the tested catalysts is shown in Figure 3b. An obvious correlation was observed, demonstrating that the catalytic activity of this system depends largely on Pt dispersion. We also focused on other factors such as the acid-base properties of the support (pH of isoelectric point as a scale); however, no correlation was observed (Figure S2). Figure 4 shows the conversion-selectivity curves obtained in PROX over several Pt₃Co catalysts. CO₂ selectivity differed slightly depending on the support and preparation method at low CO conversion. For all catalysts, the CO₂ selectivity declined upon increasing temperature and converged to 50% at full conversion. The 50% CO₂ selectivity corresponds to the 1:1 formation of CO₂ and H₂O (formally, 1:1 combustion of CO and H₂), implying the involvement of a specific reaction pathway for all catalysts. In our reaction condition, this selectivity also means that only 3% of H₂ is combusted.

Next, a kinetic study for low temperature (60°C) PROX over Pt or Pt₃Co catalysts was performed (Figure S3, the results were summarized in Table 2). A first-order dependence of O₂ pressure (P_{O_2}) and negative-order relationship with CO pressure (P_{CO}) was observed for monometallic Pt/SiO₂. This indicates that O₂ adsorption is the rate-determining step and is competitive with strong CO adsorption on Pt. In contrast, for Pt₃Co catalysts, the kinetic order of P_{O_2} was 0.79–0.85, suggesting that the rate-determining step for Pt₃Co catalysts is not O₂ adsorption, but most likely the surface reaction. Although the kinetic order of P_{CO} remains negative, the absolute values were slightly lower than that of Pt/SiO₂, implying that the competing CO adsorption was weakened in the presence of Co atoms. Based on the change in kinetics, we concluded that Co atoms, where CO adsorption is much weaker than that on Pt atoms, act as effective O₂ adsorption sites. This is also supported by the result of CO-TPD (Figure S1), where CO desorption from Co sites began at room temperature and completed below 100°C, suggesting that Co sites are open even in the low temperature PROX condition.

We then focused on the effect of H₂ on the catalytic performance and reaction mechanism. Figure 5a shows CO conversions for the Pt₃Co/MgO-catalyzed PROX reaction (CO + O₂ + excess H₂) and CO oxidation (CO + O₂) at various temperatures. The absence of H₂ resulted in significantly lower CO conversion even at high temperatures (> 120°C). Figure 5b shows changes in CO conversion during a transient experiment with H₂ on/off treatments. CO conversion decreased to the level of CO oxidation after shutting off the H₂ supply but recovered immediately after the H₂ supply was resumed. This response was repeatedly observed during the following on/off treatments, strongly suggesting an involvement of hydrogen in the catalysis of PROX. Considering the 1:1 formation of CO₂ and H₂O at high temperature region (>100°C), a reaction pathway involving CO, O₂, and H₂ in a 1:1:1 ratio, which is quite different from direct CO oxidation, is likely to occur. Note that the response of CO conversion when H₂ supply was shut off was slower than that when H₂ supply was resumed. This implies that (1) some H-containing species having long life times or high concentrations are involved in the reaction and that (2) they are immediately recovered by H₂ resumption.

We subsequently investigated the change in the surface species during PROX reaction using FT-IR to better understand the role of hydrogen. Figure 6 shows changes in FT-IR spectra during low-temperature PROX over Pt₃Co/MgO (at room temperature). An intense peak at 2088 cm⁻¹ and small shoulder at approximately 2000 cm⁻¹ were assigned to linearly adsorbed CO on Pt atoms with high (terrace) and low (edge or corner) coordination numbers, respectively.³⁰ A small amount of bridge CO was also observed at 1850 cm⁻¹.³¹ A decrease in linear CO and an increase in gas phase CO₂ at 2330 cm⁻¹ with reaction time showed that CO was converted to CO₂ at room temperature. A broad band appeared at approximately 3000–3500 cm⁻¹, corresponding to hydrogen-bonded O–H groups, suggesting H₂O evolution. The production of H₂O as a byproduct is consistent with the CO₂ selectivity less than 100% shown in Figure 4. A set of peaks observed in the region of 1000–1700 cm⁻¹ can be assigned to monodentate carbonate (1060, 1430, and 1525 cm⁻¹) and bicarbonate (1218, 1392, 1495, and 1650 cm⁻¹) species adsorbed on MgO.^{32, 33} Negative peaks were also observed at 3755 and 3530 cm⁻¹, corresponding to isolated and hydrogen-bonded surface hydroxyl groups on MgO, respectively.³⁴ Decrease in the surface hydroxyl groups implies that they are either consumed during catalysis or form strong interactions with water upon reaction. The time courses of normalized peak intensities of the

observed species are summarized in Figure 6 inset. In contrast to the monotonic increase in gaseous CO₂, adsorbed CO kept its initial value in the first stage and subsequently declined. The initial constant region corresponds to saturation coverage maintained by gas phase supply and the subsequent decrease indicates the complete consumption of gas phase CO. The peak intensity of bicarbonate decreased as the reaction proceeded, whereas those of carbonates increased. This consumption of bicarbonate can be observed clearly in the difference spectrum (12 min–10 s) as negative peaks. It should be noted that carbonates showed a monotonous increase even at the end of the reaction period. These changes indicate that bicarbonate is formed as an intermediate species of PROX reaction and that carbonates are formed as byproducts, not as intermediate species. It has been reported that carbonate species are formed by the adsorption of CO₂ on MgO.³³ Thus, in our system, a portion of the produced CO₂ seems to form carbonates upon readsorption on MgO. The time courses of CO₂ and carbonates show that carbonate formation occurs prior to the evolution of CO₂ in the gas phase. This may be because strong basic sites on MgO capture the initially formed CO₂ as a carbonate, followed by equilibration between the gaseous and adsorbed CO₂ on moderate or weak basic sites. We confirmed the presence of various basic sites on the Pt₃Co/MgO catalyst through a CO₂-TPD (Figure S4): strong (730°C), moderate (500°C, major species), and weak (250°C). The difference spectrum in Figure 6 showed a sharp negative peak at 2088 cm⁻¹, whereas almost no change was observed in the 2000 and 1850 cm⁻¹ regions, implying two types of CO adsorption sites, i.e., active (2088 cm⁻¹) and inactive (2000 and 1850 cm⁻¹), for PROX reaction. This is probably because a stronger CO adsorption, where the vibrational frequency is lowered because of enhanced back-donation, makes CO less active.

We also performed an isotope experiment to clarify the involvement of surface hydroxyl groups in the catalysis. Instead of H₂, D₂ was used for hydrogen pretreatment and/or PROX reaction. The D₂ pretreatment was performed at 400°C such that the surface hydroxyl groups on MgO were completely deuterated. Figure 7 shows the FT-IR spectra during PROX reactions at room temperature using either D₂ or H₂. H₂-treatment and D₂-reaction (hereafter, H₂→D₂) resulted in surface–OH consumption and non-deuterated bicarbonate formation (O–H bending and stretching vibrations, 1218 cm⁻¹ and 3670 cm⁻¹, respectively) at the initial stage (10 s). This strongly leads to an idea that the hydrogen atom constituting bicarbonate originated from surface hydroxyl groups, not from gas phase hydrogen. This

bicarbonate disappeared as the reaction proceeded, which is clearly shown in the difference spectrum. The newly developed peak at 1200 cm^{-1} can be assigned to DOD bending vibration of the produced D_2O .³⁵ The formation of D_2O was also demonstrated from the broad band between 2300 and 2700 cm^{-1} . The corresponding HOH bending vibration of H_2O , which has been reported to appear at 1645 cm^{-1} ,³⁶ was not clearly observed when H_2 -treatment and H_2 -reaction were performed (hereafter, $\text{H}_2 \rightarrow \text{H}_2$). This may be because of peak cancellation by an overlapping negative peak of bicarbonate at 1650 cm^{-1} , which is clearly observed in $\text{H}_2 \rightarrow \text{D}_2$ condition. It should be noted that a sharp peak appeared at 2770 cm^{-1} , which corresponds to isolated surface O–D, suggesting that the consumed surface hydroxyl groups were recovered by gas phase hydrogen and/or water. When D_2 -treatment and D_2 -reaction were performed ($\text{D}_2 \rightarrow \text{D}_2$), a decrease in surface O–D bonds was observed instead of the O–H analogs, demonstrating the H–D exchange on the surface hydroxyl groups by D_2 pretreatment. Interestingly, the O–H bending mode of the bicarbonate species was absent (1218 cm^{-1} , 10 s) despite the presence of other modes, suggesting the formation of deuterated bicarbonate.³³ This is consistent with the assumption that the bicarbonate hydrogen originated from surface hydroxyl groups. Figure 7 inset shows the change in the intensity of the bicarbonate O–H bending vibration (1218 cm^{-1}) for $\text{H}_2 \rightarrow \text{H}_2$ or $\text{H}_2 \rightarrow \text{D}_2$ condition. Although the O–H vibration was maintained for several minutes for $\text{H}_2 \rightarrow \text{H}_2$ condition, it disappeared at the beginning (1 min) for $\text{H}_2 \rightarrow \text{D}_2$ condition. This indicates that the non-deuterated bicarbonate is immediately converted to the product, followed by replacement with the deuterated bicarbonate in the latter case. As the number of surface O–H groups accessible to adsorbed CO and/or O_2 at the Pt_3Co – MgO interface is limited, the initially formed H_2O should be significantly diluted with the subsequently formed D_2O . Indeed, for $\text{H}_2 \rightarrow \text{D}_2$ condition, H_2O formation (approximately 3500 cm^{-1}) was almost negligible compared with D_2O formation (approximately 2600 cm^{-1}). These results, however, cannot exclude the possibility that the hydrogen atoms constituting water do not originate from surface hydroxyl groups but merely from gas phase hydrogen. In other words, this observation does not necessarily correspond to true catalysis, which is often indicated via spectroscopic studies. Therefore, we performed a similar experiment with sufficiently low gas content ($\text{CO}/\text{Pt} = 0.7$, $\text{CO}:\text{O}_2:\text{D}_2 = 1:1:17$) to exclude the influence of excess D_2 . Under this condition, the evolution of H_2O with CO_2 could be observed, followed by a small amount of D_2O (Figure S5). This provides strong evidence that

bicarbonate is formed as a true reaction intermediate by hydrogen supply from surface hydroxyl groups followed by decomposition to CO_2 and H_2O . We also performed in situ FT-IR measurements in PROX at a higher reaction temperature (100°C). Bicarbonate and carbonate were formed along with H_2O and CO_2 (Figure S6), similar to Figure 6. However, spectral change over time (Figure 8) differed slightly from that at room temperature (Figure 6 inset). CO_2 formation reached near saturation at the beginning (14 s), as is consistent with the significantly higher CO conversion. Adsorbed CO did not reach saturation coverage at the initial stage (14 s–3 min), which was followed by saturation and a subsequent decrease. This is most likely because of weaker CO adsorption at higher temperature, suggesting that the competitive adsorption of O_2 and/or H_2 is allowed. Bicarbonate gradually decreased compared with the drastic increase in CO_2 , indicating another reaction pathway that is independent of surface-OH-derived bicarbonate. A possible interpretation is that a Langmuir–Hinshelwood-type reaction between the adsorbed CO, O_2 , and H_2 (or H) occurs on the Pt_3Co surface, as well as that involving surface OH at the Pt_3Co – MgO interface.

Based on these results, a plausible reaction mechanism is proposed, as shown in Scheme 1. CO molecules are adsorbed on surface Pt and Co atoms, with adsorption on Co being weak, allowing for O_2 adsorption on the catalyst surface. The presence of such effective O_2 adsorption sites changes the rate-determining step from O_2 adsorption to surface reaction. At low temperature regions, CO is converted to bicarbonate intermediate by reacting with O_2 and hydrogen derived from surface hydroxyl groups at the Pt_3Co – MgO interface (Scheme 1a). The formed bicarbonate is decomposed to CO_2 and H_2O by receiving another hydrogen atom. This decomposition step may be the rate-determining step at low temperature regions as bicarbonate can be detected, i.e., its decomposition should be slower than its formation. Hydrogen supply from surface hydroxyl groups can be mediated in a reverse spillover fashion by Pt or, more simply, by proton migration. A portion of CO_2 is captured by MgO as carbonate. The consumed surface hydroxyl groups are recovered through spillover hydrogen or byproduct water. This reaction pathway yields CO_2 and H_2O in essentially a 1:1 ratio, i.e., 50% CO_2 selectivity. It should be noted that an increase in temperature weakens CO adsorption (Scheme 1b), enhancing O_2 adsorption and accelerating the overall reaction rate. Weaker CO adsorption also enables H_2 dissociation and hydrogen supply on Pt sites such that some intermediate is formed without the aid of surface OH. The

reaction pathway via a bicarbonate-like intermediate is consistent stoichiometrically with the CO₂ selectivity converged to 50% at high temperature (Figure 4, >100°C). In this context, assuming a formate-like intermediate as mentioned in the next paragraph does not agree with the stoichiometry. Greater than 50% CO₂ selectivity at low temperature (60–80°C, corresponding to 20%–40% CO conversion, Figure 4) may be because the byproduct water is used for the regeneration of surface hydroxyl groups. The contribution of direct CO oxidation would also be involved. Thus, surface hydroxyl groups play an important role in the reaction mechanism by generating the bicarbonate intermediate. This reaction mechanism is also consistent with the CO conversion response in the transient H₂ on-off experiment shown in Figure 5b. The slow response in H₂ shutting off may be attributed to the consumption of surface hydroxyl group and the residual adsorbed water as hydrogen sources for low temperature PROX. The H₂ resumption immediately allows the H-involved reaction pathways to recover the original CO conversion.

Finally, we summarize the two noteworthy features of this study and discuss the difference between our intermetallic system and other catalytic systems. First, this is the first example of spectroscopic evidence of a bicarbonate intermediate in PROX. Among a number of Pt-based PROX catalytic systems, only one research group has reported spectroscopic evidence for a reaction intermediate. Tanaka et al. proposed that formate species (HCOO) were formed as reaction intermediates from adsorbed CO and migrating OH⁻ anions in PROX over a FeO_x-modified Pt/TiO₂ catalyst.^{37, 38} Formate species adsorbed on MgO typically show an OCO symmetric stretching vibration in the 1280–1360 cm⁻¹ region,³⁹ which is clearly distinguishable from the O–H bending vibration of bicarbonate at ca. 1220 cm⁻¹. In Figure 6, a very small peak observed at 1280 cm⁻¹ might be assignable to formate. However, no spectral change was observed during the PROX reaction, indicating that its contribution to catalysis is negligible. Second, surface hydroxyl groups play an important role in PROX. Although some researchers investigated the involvement of surface hydroxyl groups in PROX, the reaction mechanism differs from that of our system. Fukuoka et al. reported that surface hydroxyl groups on Pt/FSM-16 were highly reactive toward CO adsorbed on Pt nanoparticles at the interface of Pt and FSM-16.⁴⁰ However, the CO–CO₂ conversion fashion (CO + –OH → CO₂ + 1/2 H₂) was entirely different from that proposed in our study and reaction intermediates were not discussed. Similar

involvement of surface hydroxyl groups has also been proposed for Pt/CeO₂ catalyst; however, surface hydroxyl group reacts directly with adsorbed CO to convert into formate intermediate.^{41, 42} Thus, the present study proposes a novel and unique reaction mechanism of PROX with strong spectroscopic evidence. This unique reaction pathway stems from the presence of the Pt–Co support double interface as an effective reaction site for association of CO, O₂, and H at low temperature.

Conclusion

In this study, the reaction mechanism and intermediate behavior in PROX over Pt₃Co intermetallic catalysts supported on various oxides (SiO₂, Al₂O₃, MgO, CaO, and La₂O₃) were investigated in detail. The nature of the support and preparation method affects the Pt₃Co particle size and Pt dispersion. CO conversion depends strongly on Pt dispersion, but not on the acid–base properties of the support. Pt₃Co/MgO demonstrated the highest catalytic activity (97% CO conversion and 50% CO₂ selectivity at 100°C) among the tested catalysts. Co atoms act as effective O₂ adsorption sites. At low temperature (< 60°C), a bicarbonate species is formed as a reaction intermediate from adsorbed CO, O₂, and surface hydroxyl groups at the Pt₃Co-support interface, followed by decomposition to CO₂ and H₂O. At high temperature (> 80°C), H₂ activation at Pt sites occurs to enable bicarbonate-like intermediate formation without the aid of surface hydroxyl groups. These reaction pathways generate CO₂ and H₂O in a 1:1 ratio, i.e., 50% CO₂ selectivity. The present study provides the first spectroscopic evidence of bicarbonate formation as an intermediate in PROX and the involvement of surface hydroxyl groups in its formation. In addition, the proposed reaction mechanism is unique compared with those reported for other PROX systems.

Acknowledgement

This work was supported by JSPS KAKENHI Grant Number 26820350. We deeply appreciate Center for Advanced Materials Analysis Tokyo Institute of Technology for the aid of TEM observation.

References

- 1 A. F. Ghenciu, *Curr. Opin. Solid State Mater. Sci.*, 2002, **6**, 389-399.

- 2 J. L. Ayastuy, M. P. Gonzalez-Marcos, J. R. Gonzalez-Velasco and M. A. Gutierrez-Ortiz, *Appl. Catal. B: Environ.*, 2007, **70**, 532-541.
- 3 K. I. Tanaka, M. Shou, H. He and X. Y. Shi, *Catal. Lett.*, 2006, **110**, 185-190.
- 4 M. Kotobuki, A. Watanabe, H. Uchida, H. Yamashita and M. Watanabe, *Appl. Catal. A: Gen.*, 2006, **307**, 275-283.
- 5 H. Zhang, X. J. Liu, N. W. Zhang, J. B. Zheng, Y. P. Zheng, Y. H. Li, C. J. Zhong and B. H. Chen, *Appl. Catal. B: Environ.*, 2016, **180**, 237-245.
- 6 M. Kotobuki, A. Watanabe, H. Uchida, H. Yamashita and M. Watanabe, *J. Catal.*, 2005, **236**, 262-269.
- 7 M. Watanabe, H. Uchida, K. Ohkubo and H. Igarashi, *Appl. Catal. B: Environ.*, 2003, **46**, 595-600.
- 8 J. A. H. Dreyer, H. K. Grossmann, J. F. Chen, T. Grieb, B. B. Gong, P. H. L. Sit, L. Madler and W. Y. Teoh, *J. Catal.*, 2015, **329**, 248-261.
- 9 H. Zhang, D. R. Lin, G. T. Xu, J. B. Zheng, N. W. Zhang, Y. H. Li and B. H. Chen, *Int. J. Hydrogen Energy*, 2015, **40**, 1742-1751.
- 10 H. L. Li, X. H. Yu, S. T. Tu, J. Y. Yan and Z. D. Wang, *Appl. Catal. A: Gen.*, 2010, **387**, 215-223.
- 11 C. Wang, B. D. Li, H. Q. Lin and Y. Z. Yuan, *J. Power Sources*, 2012, **202**, 200-208.
- 12 E. Y. Ko, E. D. Park, H. C. Lee, D. Lee and S. Kim, *Angew. Chem. Int. Ed.*, 2007, **46**, 734-737.
- 13 P. V. Snytnikov, K. V. Yusenko, S. V. Korenev, Y. V. Shubin and V. A. Sobyenin, *Kinet. Catal.*, 2007, **48**, 276-281.
- 14 T. Komatsu and A. Tamura, *J. Catal.*, 2008, **258**, 306-314.
- 15 T. Moriya, J. Kugai, S. Seino, Y. Ohkubo, T. Nakagawa, H. Nitani and T. A. Yamamoto, *J. Nanopart. Res.*, 2013, **15**, 1-8.
- 16 J. Kugai, R. Kitagawa, S. Seino, T. Nakagawa, Y. Ohkubo, H. Nitani, H. Daimon and T. A. Yamamoto, *Appl. Catal. A: Gen.*, 2011, **406**, 43-50.
- 17 J. Kugai, T. Moriya, S. Seino, T. Nakagawa, Y. Ohkubo, H. Nitani, Y. Mizukoshi and T. A. Yamamoto, *Appl. Catal. B: Environ.*, 2012, **126**, 306-314.
- 18 S. Lang, M. Turk and B. Kraushaar-Czarnetzki, *J. Catal.*, 2012, **286**, 78-87.
- 19 E. Y. Ko, E. D. Park, K. W. Seo, H. C. Lee, D. Lee and S. Kim, *Catal. Lett.*, 2006, **110**, 275-279.
- 20 S. J. Huang, K. Hara and A. Fukuoka, *Energ. Environ. Sci.*, 2009, **2**, 1060-1068.
- 21 J. L. Ayastuy, A. Gil-Rodriguez, M. P. Gonzalez-Marcos and M. A. Gutierrez-Ortiz, *Int. J. Hydrogen Energy*, 2006, **31**, 2231-2242.
- 22 E. O. Jardim, S. Rico-Frances, F. Coloma, J. A. Anderson, J. Silvestre-Albero and A. Sepulveda-Escribano, *J. Colloid Interface Sci.*, 2015, **443**, 45-55.
- 23 S. Rico-Frances, E. O. Jardim, T. A. Wezendonk, F. Kapteijn, J. Gascon, A. Sepulveda-Escribano and E. V. Ramos-Fernandez, *Appl. Catal. B: Environ.*, 2016, **180**, 169-178.
- 24 A. Wootsch, C. Descorme and D. Duprez, *J. Catal.*, 2004, **225**, 259-266.

- 25 T. M. Pedersen, W. X. Li and B. Hammer, *Phys. Chem. Chem. Phys.*, 2006, **8**, 1566-1574.
- 26 L. Vitos, A. V. Ruban, H. L. Skriver and J. Kollar, *Surf. Sci.*, 1998, **411**, 186-202.
- 27 V. R. Stamenkovic, B. S. Mun, M. Arenz, K. J. J. Mayrhofer, C. A. Lucas, G. F. Wang, P. N. Ross and N. M. Markovic, *Nat. Mater.*, 2007, **6**, 241-247.
- 28 Y. Xu, A. V. Ruban and M. Mavrikakis, *J. Am. Chem. Soc.*, 2004, **126**, 4717-4725.
- 29 R. P. Galhenage, H. Yan, A. S. Ahsen, O. Ozturk and D. A. Chen, *J. Phys. Chem. C*, 2014, **118**, 17773-17786.
- 30 M. J. Kappers and J. H. Vandermaas, *Catal. Lett.*, 1991, **10**, 365-373.
- 31 M. R. McClellan, J. L. Gland and F. R. Mcfeeley, *Surf. Sci.*, 1981, **112**, 63-77.
- 32 D. Cornu, H. Guesmi, J. M. Krafft and H. Lauron-Pernot, *J. Phys. Chem. C*, 2012, **116**, 6645-6654.
- 33 J. V. Evans and T. L. Whateley, *T. Faraday Soc.*, 1967, **63**, 2769-2777.
- 34 C. Chizallet, G. Costentin, M. Che, F. Delbecq and P. Sautet, *J. Am. Chem. Soc.*, 2007, **129**, 6442-6452.
- 35 E. Catalano and D. E. Milligan, *J. Chem. Phys.*, 1959, **30**, 45-47.
- 36 Y. Y. Liu, K. Suzuki, S. Hamakawa, T. Hayakawa, K. Murata, T. Ishii and M. Kumagai, *Catal. Lett.*, 2000, **66**, 205-213.
- 37 K. I. Tanaka, M. Shou and Y. Z. Yuan, *J. Phys. Chem. C*, 2010, **114**, 16917-16923.
- 38 X. Y. Shi, K. Tanaka, H. He, M. S. Shou, W. Q. Xu and X. L. Zhang, *Catal. Lett.*, 2008, **120**, 210-214.
- 39 T. Shido, K. Asakura and Y. Iwasawa, *J. Catal.*, 1990, **122**, 55-67.
- 40 A. Fukuoka, J. I. Kimura, T. Oshio, Y. Sakamoto and M. Ichikawa, *J. Am. Chem. Soc.*, 2007, **129**, 10120-10125.
- 41 O. Pozdnyakova, D. Teschner, A. Wootsch, J. Krohnert, B. Steinhauer, H. Sauer, L. Toth, F. C. Jentoft, A. Knop-Gericke, Z. Paal and R. Schlogl, *J. Catal.*, 2006, **237**, 1-16.
- 42 C. Li, Y. Sakata, T. Arai, K. Domen, K. I. Maruya and T. Onishi, *J. Chem. Soc. Faraday Trans. 1*, 1989, **85**, 1451-1461.

Tables

Table 1. Size of Pt₃Co nanoparticles supported on various oxides and their Pt dispersion.

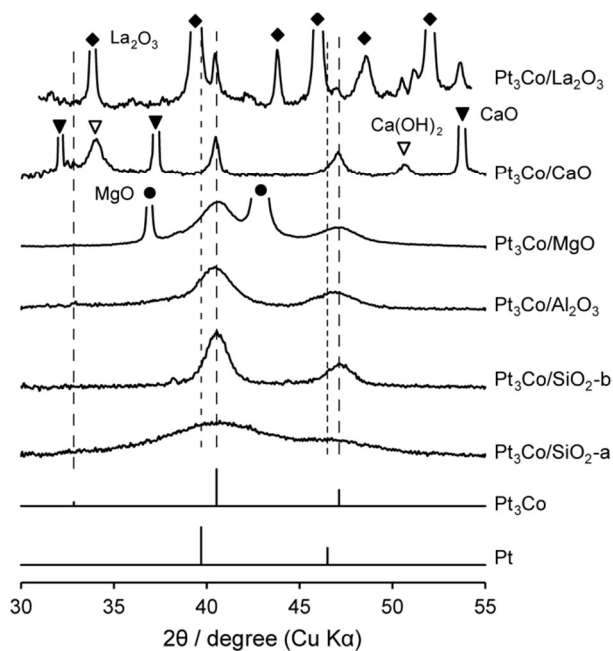
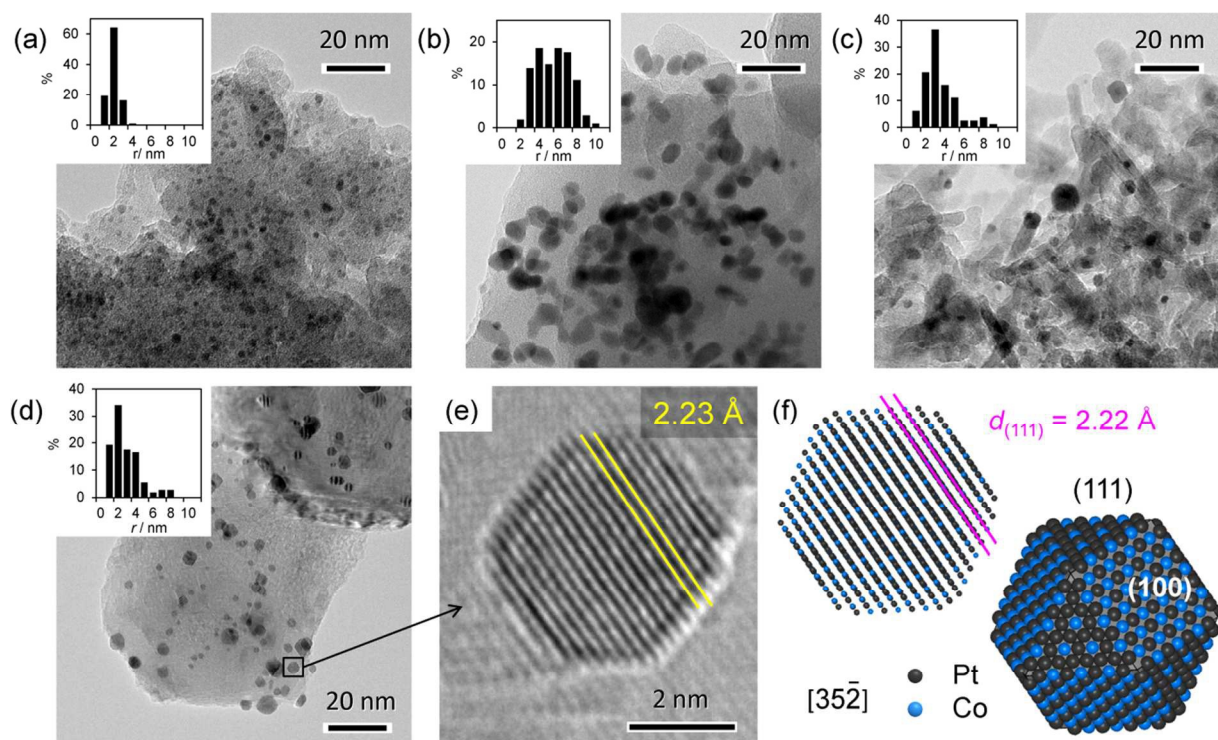
support	S_{BET} /m ² g ⁻¹	d_{XRD} / nm ^a	d_{TEM} / nm ^b	D_{CO} (%) ^c	D_{TEM} (%) ^d
SiO ₂ -a	500	2	2.8	11.7	16.4
SiO ₂ -b	500	7	7.4	3.6	8.7
Al ₂ O ₃	270	6	6.2	13.5	10.0
MgO	33	6	6.0	16.0	10.3
CaO	37	18	–	0.86	–
La ₂ O ₃	2	30	–	0.27	–

^a Crystallite size estimated by the Scherrer equation. ^b Volume average particle size obtained from TEM analysis. ^c Pt dispersion determined by CO chemisorption. ^d Pt dispersion estimated by the cuboctahedron model with d_{TEM} .

Table 2. Reaction order of reactant pressure on CO₂ formation rate in PROX (60°C) over Pt and Pt₃Co catalysts.

catalyst	P_{CO}	P_{O_2}
Pt/SiO ₂	-1.42	1.08
Pt ₃ Co/SiO ₂ -a	-1.39	0.84
Pt ₃ Co/Al ₂ O ₃	-1.29	0.79
Pt ₃ Co/MgO	-1.27	0.85

Figures

Figure 1. XRD patterns of Pt₃Co catalysts.Figure 2. TEM images and size distribution of Pt₃Co nanoparticles supported on (a) SiO₂-a, (b) SiO₂-b, (c) Al₂O₃, and (d) MgO. (e) High-resolution TEM image of a single nanoparticle designated by the small square in (d). (f) Cuboctahedron models of intermetallic Pt₃Co nanocrystals projected along the [35-2] direction with small-ball (left) and space-filling (right) models.

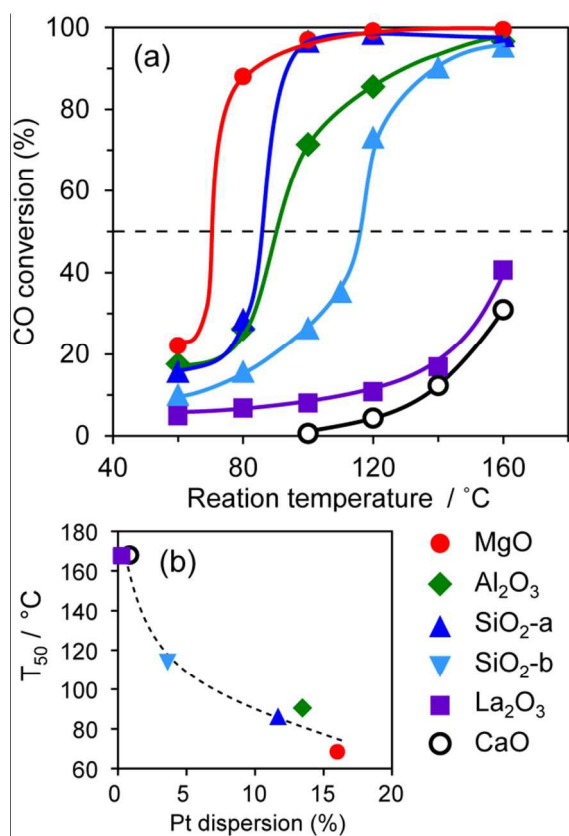


Figure 3. (a) Temperature dependence of CO conversion in PROX over various Pt₃Co/MO_x catalysts (MO_x is indicated by symbols) and (b) relationship between the T_{50} and Pt dispersions.

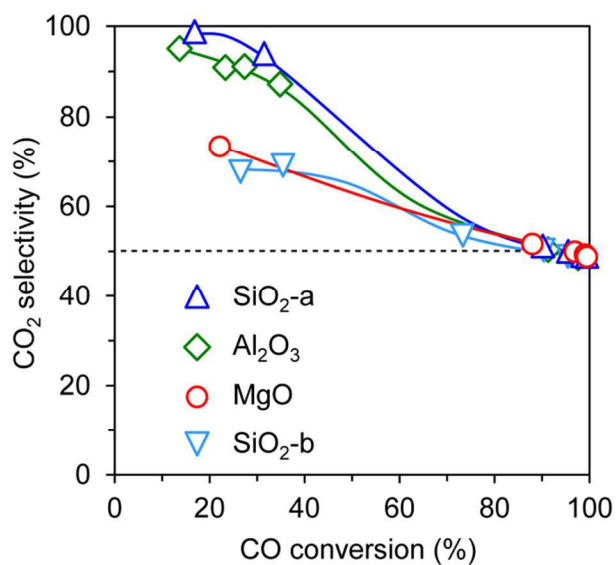


Figure 4. Conversion-selectivity curves for PROX over various Pt₃Co/MO_x catalysts.

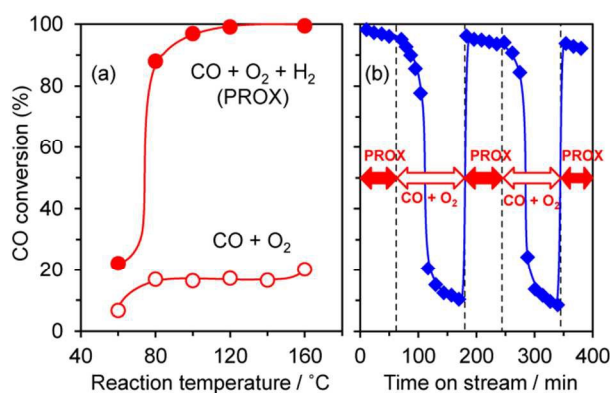


Figure 5. (a) Temperature dependence of CO conversion in PROX ($\text{CO} + \text{O}_2 + \text{H}_2$) and CO oxidation ($\text{CO} + \text{O}_2$) over $\text{Pt}_3\text{Co}/\text{MgO}$ and (b) change in CO conversion in the presence and absence of H_2 at 100°C .

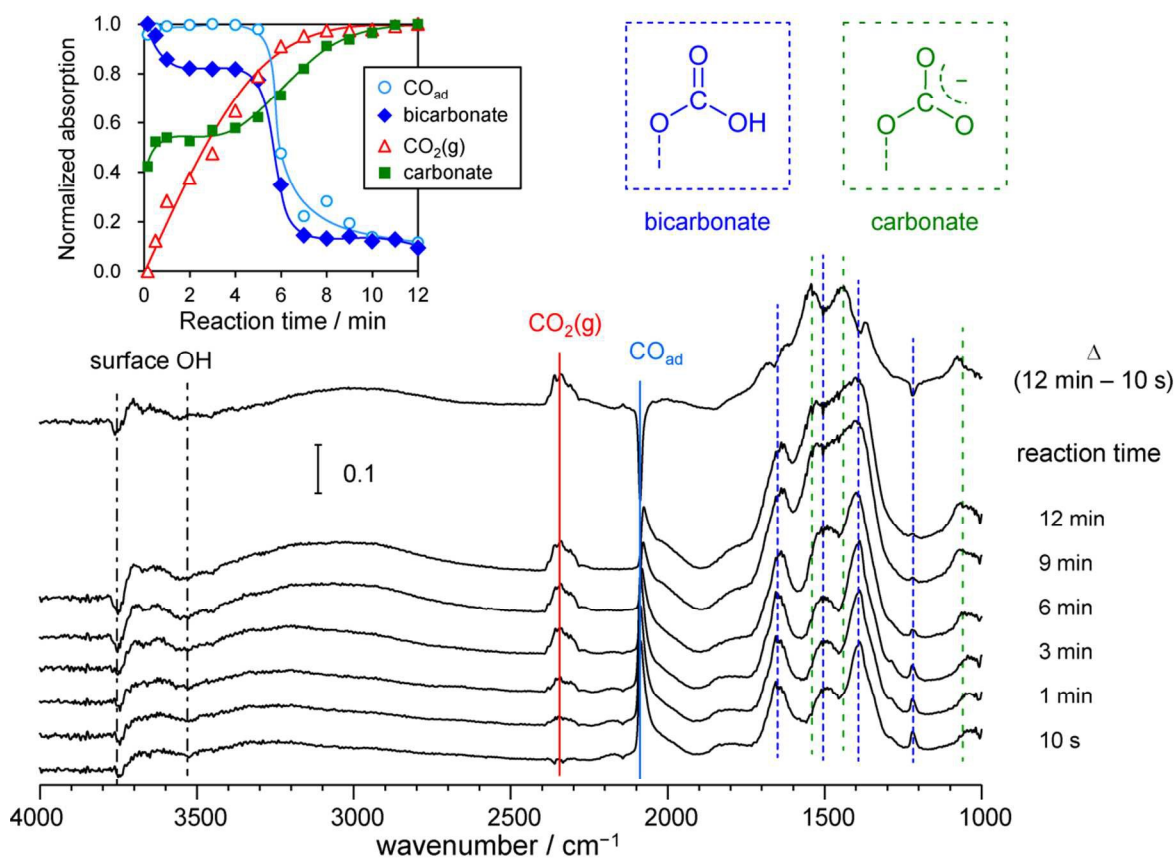


Figure 6. FT-IR spectra during low-temperature PROX over $\text{Pt}_3\text{Co}/\text{MgO}$ (at room temperature). Inset shows the time courses of normalized peak intensity for relevant species.

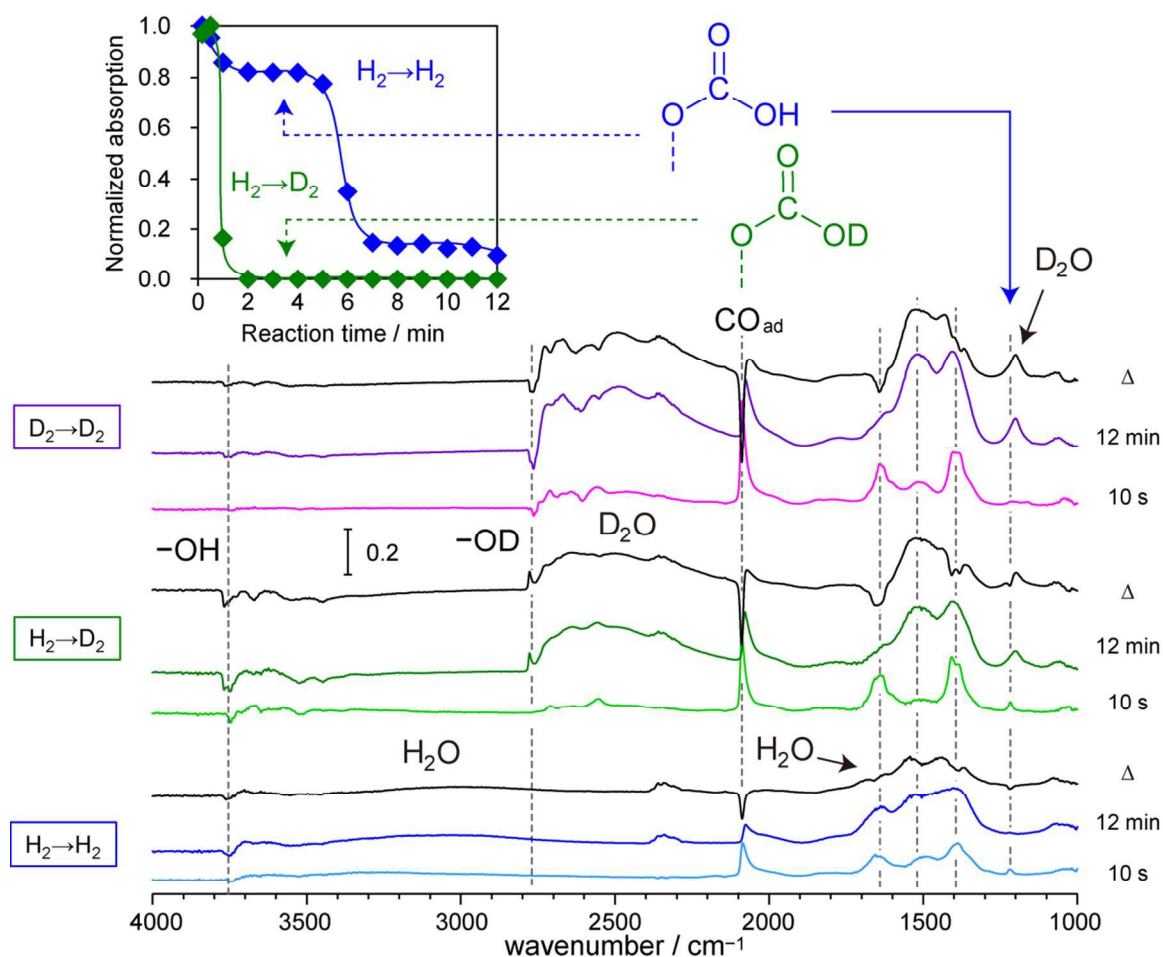


Figure 7. FT-IR spectra during low-temperature PROX over Pt₃Co/MgO with H₂(D₂) pretreatment and H₂(D₂) feeding, designated as H₂(D₂)→H₂(D₂). Inset shows time courses of normalized peak intensity at 1218 cm⁻¹, corresponding to the O-H bending mode of bicarbonate.

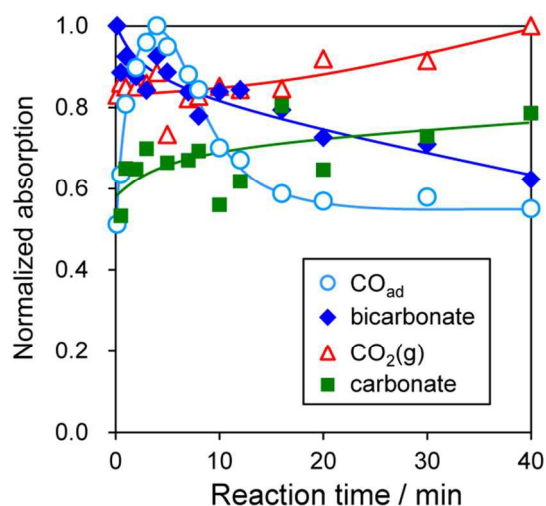
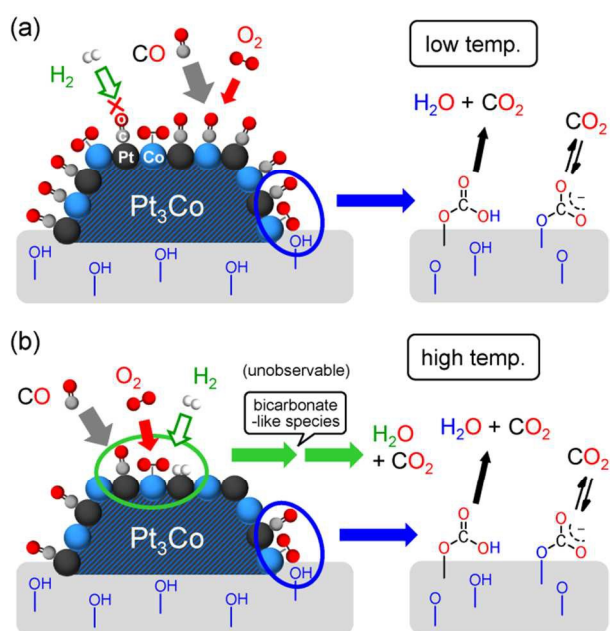
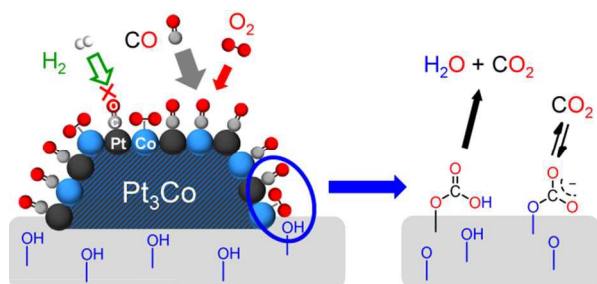


Figure 8. Changes in normalized intensities of FT-IR bands observed during high-temperature PROX (100°C).



Scheme 1. Proposed reaction mechanisms of PROX over Pt₃Co on an oxide support at (a) low and (b) high temperature regions.

Table of Contents Image



Textual abstract

Unique and novel reaction mechanism of preferential oxidation of CO involving surface-OH-derived bicarbonate as an intermediate is reported